Jurnal Fisika 16 (1) (2026) 47-62
Jurnal Fisika
https://journal.unnes.ac.id/nju/index.php/jf/index

Comparative Analysis Of MRI Image Classification Methods Based On Texture Features For Brain Tumor Detection Using Random Forest

Delia Okta Rahmadani*, Moch. Husain, Akmal K.H., Heni Sumarti

Departement of Physics, Faculty of Science and Technology, Universitas Islam Negeri Walisongo Semarang, Indonesia

Article Info

Article History:

Received:
18 December 2025

Accepted:
20 April 2026

Published:
15 May 2026

Keywords:
MRI, image texture, glioma, meningioma, pituitary, classfication, Random Forest.

Abstract

Medical personnel struggle to detect brain tumors including glioma and meningioma and pituitary tumors because these tumors display matching MRI features which produces different interpretation results between different observers. The research aims to identify three brain tumor types by analyzing MRI image textures and it assesses different classification methods. The Weka software analyzed 3,900 MRI images through Histogram and Gray Level Co-occurrence Matrix (GLCM) and GLRLMGray Level Run Length Matrix (GLRLM) feature extraction methods before Support Vector Machine (SVM)[SF1.1][A1.2] and Naive Bayes and Multilayer Perceptron and Multiclass Classifier and Random Forest algorithms conducted the classification tasks. The analysis revealed that each tumor pair possesses distinct dominant texture characteristics which consist of standard deviation for glioma–meningioma and energy for glioma–pituitary and homogeneity for meningioma–pituitary. The Random Forest algorithm achieved the best classification results in all experiments because it reached 88.62% accuracy for glioma–meningioma and 96.96% accuracy for glioma–pituitary and 95.92% accuracy for meningioma–pituitary while maintaining high sensitivity and specificity values. The research demonstrates that brain tumor MRI image identification becomes more accurate through the combination of texture features with Random Forest classification methods which leads to better medical diagnostic results.

✉ Correspondence address:
Departement of Physics, Faculty of Science and Technology, Universitas Islam Negeri Walisongo Semarang, Indonesia
E-mail: dely.aarhm@gmail.com

p-ISSN 2088-1509

INTRODUCTION

Brain tumors develop as abnormal cell growths which occur inside the intracranial space and they can either develop independently or spread from different body organs. Brain tumors which appear benign through histological examination can still cause dangerous effects because they exist near essential neural structures. Brain tumors develop through genetic elements which combine with DNA mutations that trigger abnormal cell growth and radiation exposure and specific chemical substances that modify gene arrangements. The exact origins of most benign brain tumors continue to remain unidentified despite current medical knowledge. The symptoms of brain tumors depend on their dimensions and their position in the brain because they start with headaches and fatigue before causing seizures and increased intracranial pressure and specific brain function impairment through tissue compression (Heranurweni et al., 2018).

Medical professionals need to identify three brain tumor types which include glioma and meningioma and pituitary tumors because these tumors show identical visual patterns during medical imaging procedures. Medical experts who perform manual interpretation face the challenge of subjective decision-making because their clinical experience affects their diagnostic results which produce inconsistent results. The challenge demonstrates that healthcare needs better detection systems which would minimize the uncertainty that occurs when doctors try to identify tumor types. (Wardhani & Nafi'iyah, 2023).

One effective way to detect brain tumors is by using digital Magnetic Resonance Imaging (MRI) techniques. The medical field uses MRI as its primary tool for brain tumor diagnosis because this imaging technique produces detailed brain structure pictures which help doctors detect brain tumors (Salman et al., 2025). The fundamental principle of Magnetic Resonance Imaging involves using computer systems with magnetic fields ranging from 0.064 to 7.0 Tesla and radiofrequency waves to produce medical images. The system produces human body cross-sectional images through its combined operation. MRI stands out because it operates with non-ionizing radiation which provides patients with safer imaging compared to other available methods. The system operates without needing any surgical methods to produce detailed soft tissue images. MRI technology enables users to view the human body through different perspectives which include transversal and sagittal and coronal and oblique views. This results in more detailed and clearer anatomical representations (Maulida et al., 2019). But here's the catch: even though MRI images are packed with visual information, analyzing them still heavily depends on human interpretation, which can lead to mistakes.

The development of multiple digital image processing techniques exists as solutions which help solve the problems that occur during MRI image interpretation. The analysis of MRI images and histogram analysis and GLCM and GLRLM represent the main methods which researchers use for their studies. A histogram displays the number of times each gray-level intensity value appears in an image. A histogram displays gray-level intensity values on its x-axis while its y-axis shows how often these values appear (Kusuma & Kusumadewi, 2020). The Gray Level Co-occurrence Matrix (GLCM) shows how pixel intensity values in an image relate to each other through their spatial positions. Several texture features, such as contrast, homogeneity, energy, correlation, and entropy, are incorporated into this method (Sofian & Laluma, 2019). One technique for differentiating between fine and coarse textures in texture analysis is the Gray Level Run Length Matrix (GLRLM). Short Run Emphasis (SRE), Long Run Emphasis (LRE), Gray Level Uniformity (GLU), and Run Length Uniformity (RLU) are texture features that are obtained from GLRLM (Astiningrum et al., 2020).

The three methods Histogram and GLCM and GLRLM have proven useful for feature extraction in multiple research studies yet they face challenges when integrated with contemporary classification systems to enhance brain tumor classification precision. The current research lacks a

complete assessment of different classification algorithms because it focuses on individual algorithms and specific texture features for brain tumor identification.

The research uses Support Vector Machine (SVM) and Naive Bayes and Multilayer Perceptron and Multiclass Classifier and Random Forest algorithms to classify brain tumor MRI images through the combination of texture features from Histogram and GLCM and GLRLM characteristics. The proposed combination will produce superior classification results which will help scientists understand how texture characteristics influence model performance when identifying pituitary tumors and gliomas and meningiomas. The research establishes which classification methods produce the most effective results for MRI texture data obtained through extraction methods.

The research gap in the existing literature lies in the absence of a systematic comparative study that simultaneously evaluates multiple classification algorithms—including SVM, Naive Bayes, Multilayer Perceptron, Multiclass Classifier, and Random Forest—using a combination of first-order (Histogram) and second-order (GLCM and GLRLM) texture features for pairwise classification of three brain tumor types (glioma, meningioma, and pituitary). Previous studies such as Laksono et al. (2023) and Tarigan et al. (2025) evaluated only single algorithms and limited feature sets, making cross-algorithm performance comparison difficult. The contribution of this study is threefold: (1) it provides a comprehensive assessment of five classification algorithms under identical experimental conditions using 3,900 MRI images, (2) it identifies the most discriminative texture feature for each tumor pair through attribute ranking, and (3) it demonstrates that Random Forest combined with multi-method texture extraction achieves competitive classification performance, offering a foundation for objective computer-aided diagnostic tools in brain tumor identification.

Research has used GLCM feature extraction together with the Naïve Bayes algorithm to detect brain tumors from MRI data which achieved its highest detection rate of 80% when using 80 images for training and 20 images for testing from a total of 253 images. The research benefits from its extensive data collection and its threefold evaluation method which produces measurable results and its development of a web-based system for implementation. The system has three main restrictions because it uses only a few GLCM features which do not effectively represent tumor texture complexity and the Naïve Bayes algorithm fails to handle data with feature correlations and human labeling creates potential bias in the results (Laksono et al., 2023).

The research employed SVM classification together with GLCM feature extraction to develop an automated brain tumor detection system which processed 900 MRI images. The model achieved 97.77% accuracy while showing 95% sensitivity and 99.16% specificity in its output which matched the results of radiologists exactly. The study achieved better outcome reliability through its extensive data collection and its implementation of K-Fold cross-validation for validation and its ability to verify results against radiology expert assessments. The system contains three major weaknesses because it uses downscaling which hides essential structural details and requires images from one institution and lacks evaluation of deep learning methods that could generate superior results (Tarigan et al., 2025).

METHOD

Data Collection

An open-access brain tumor MRI image dataset that has been extensively utilized in related research was used for data collection in this study. MRI pictures classified by tumor types, such as pituitary, meningioma, and glioma, are included in the dataset. Without any further preprocessing, every image was gathered in its original format as supplied by the dataset. In order to make feature extraction easier in the next stage of analysis, the images were subsequently saved and arranged into folders based on tumor class. The overall research flowchart is shown in Figure 1.

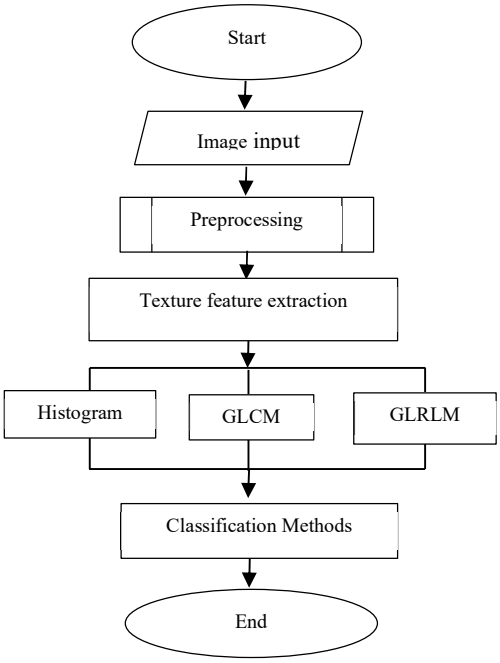

Figure 1. Research flowchart

Image Processing

The image processing method in this study involved converting brain tumor MRI images obtained from https://www.scidb.cn/en/detail?dataSetId=faa44e0a12da4c11aeee91cc3c8ac11e. From the entire dataset, only 1,300 images were selected for each tumor type (glioma, meningioma, and pituitary). Texture feature extraction was then used to immediately translate these images into numerical data. The Google Colab platform's Python programming language was used to process every MRI image. The images were read in their original format at this point, and the Histogram, GLCM, and GLRLM techniques were used to extract texture values. Using existing image processing and texture analysis libraries, the extraction process produced a set of numerical parameters that represented each tumor's texture characteristics. A feature dataset that was prepared for use in the classification stage was created by organizing all of the generated numerical values into tables.

Mean, variance, standard deviation (std), skewness, kurtosis, and entropy are among the features of the extracted histogram. An image's overall intensity level is indicated by the mean, which is the average or central value. The degree of variation or heterogeneity within an image histogram is measured by variance. The data's deviation from the mean is measured by the standard deviation. The relative asymmetry of an image's histogram curve is indicated by skewness. Kurtosis is a measure of the histogram curve's relative peakiness. The degree of disorder or randomness in an image's structure is represented by entropy (Andono et al., 2018).

$$Mean\ (\mu) = \sum_{k=0}^{L-1} kp(k) \tag{1}$$

$$Variance\ (\sigma^2) = \sum_{k=0}^{L-1} (k-\mu)^2 p(k) \tag{2}$$

$$Standard\ Deviation\ (\sigma) = \sqrt{\sigma^2} \tag{3}$$

$$Skewness\ (\gamma_1) = \frac{1}{\sigma^3}\sum_{k=0}^{L-1}(k-\mu)^3 p(k) \tag{4}$$

$$Kustosis\ (\gamma_2) = \frac{1}{\sigma^4}\sum_{k=0}^{L-1}(k-\mu)^4 p(k) \tag{5}$$

$$Entropy\ (H) = \sum_{k=0}^{L-1} p(k) log_2 p(k) \tag{6}$$

Contrast, correlation, energy, and homogeneity are among the GLCM features that were extracted. Contrast quantifies the spatial frequency of the image and variations in GLCM moments by measuring the presence of variations in pixel gray levels within an image. The degree of linear dependence between the image's gray-level values is represented by correlation. The concentration of particular gray-level intensity pairs within the matrix is indicated by energy. The uniformity of intensity variations in an image is measured by homogeneity (Sofian & Laluma, 2019).

$$Contrast = \sum_i \sum_j (i-j)^2 P(i,j) \tag{7}$$

$$Correlation = \sum_i \sum_j \frac{(i-\mu_i)(j-\mu_j)P(i,j)}{\sigma_i \sigma_j} \tag{8}$$

$$Energy = \sum_i \sum_j P(i,j)^2 \tag{9}$$

$$Homogenity = \sum_i \sum_j \frac{P(i,j)^2}{1+|i-j|} \tag{10}$$

Short Run Emphasis (SRE), Long Run Emphasis (LRE), Gray Level Non-Uniformity (GLN), Run Length Non-Uniformity (RLN), and Run Percentage (RP) are among the GLRLM features that were extracted. The predominance of short runs, which correspond to finer textures, is indicated by SRE. The predominance of long runs, which indicate coarser textures, is reflected in LRE. Higher values of GLN indicate more non-uniformity in the distribution of gray-level intensities. Run length variation is quantified by RLN, with higher values denoting greater run length variability. RP calculates the ratio of runs to all pixels in a given direction (Astiningrum et al., 2020).

$$SRE = \frac{\sum_i \sum_j \frac{R(i,j)}{j^2}}{\sum_i \sum_j R(i,j)} \tag{11}$$

$$LRE = \frac{\sum_i \sum_j j^2 R(i,j)}{\sum_i \sum_j R(i,j)} \tag{12}$$

$$GLN = \frac{\sum_i (\sum_j R(i,j))^2}{\sum_i \sum_j R(i,j)} \tag{13}$$

$$GLN = \frac{\sum_j (\sum_i R(i,j))^2}{\sum_i \sum_j R(i,j)} \tag{14}$$

$$RP = \frac{\sum_{i=1}^{N_g} \sum_{j=1}^{N_r} R(i,j)}{N_p} \tag{15}$$

Attribute Ranking

In this study, attribute ranking was used to assess each texture feature's level of contribution to the differentiation of brain tumour types in MRI images. By identifying the most pertinent characteristics, this procedure seeks to shed light on the characteristics that have the greatest impact on the classification process.

ReliefAttributeEval with the Ranker technique in the WEKA software was used for the ranking process. Relief assesses each attribute according to how well it can distinguish samples from various classes while preserving consistency for samples in the same class. This method gives higher weights to characteristics that show significant differences between classes but stay mostly constant within the same class.

$$W(A_j) = \frac{1}{m} \sum_{i=1}^{m} \left[diff(A_j, x_i, NearMiss_i) - diff(A_j, x_i, NearHit_i) \right] \tag{16}$$

Relief determines the separation between each sample and its closest neighbour from both the same class (near hit) and a different class (near miss) during the evaluation process. The attribute weights are updated iteratively based on the difference in these distances. For class differentiation, characteristics that increase the distance to near misses while decreasing the distance to near hits are thought to be more informative.

The Ranker method is used to rank the attributes in descending order of their weights after all of the attributes' weights have been determined. As the most important characteristics in the classification process, attributes with the highest weights are positioned at the top of the ranking. On the other hand, characteristics with lower weights are thought to be less significant and might be removed or given less importance in subsequent research.

The ranking's findings show that different types of brain tumours are distinguished by different texture characteristics. Certain feature combinations produce better classification performance during testing, which may be explained by the more dominant contributions of some attributes. As a result, attribute ranking functions as a basis for both feature selection and the interpretation of the MRI texture features that are pertinent to classification.

Classification

Numerical data from the extraction of texture features from MRI images of brain tumours were used in this study's classification method. Weka software was used to process all of the features obtained from the Histogram, Grey Level Co-occurrence Matrix (GLCM), and Grey Level Run Length Matrix (GLRLM) into a single dataset. Several classification models were constructed and assessed using this dataset in order to compare how well each algorithm performed in identifying different types of brain tumours.

Algoritma Support Vector Machine (SVM) is one of the Because it can create the best decision boundaries between classes, the Support Vector Machine (SVM) algorithm was used as one of the classification techniques. In order to find a hyperplane that divides data from two or more classes with the greatest margin, SVM maps the data into a higher-dimensional space. The degree to which MRI texture features can be optimally separated in both linear and nonlinear feature spaces was investigated in this study using SVM.

$$f_c(x) = w_c^t \phi(x) + b_c \tag{17}$$

Using Bayes' Theorem and the presumption that each feature is independent of the others, Naive Bayes was used as a probabilistic classification technique. This algorithm uses the distribution of a data instance's features to determine the likelihood that it belongs to a specific class. Naive Bayes was used as a benchmark because of its ease of use and computational efficiency, even though the independence assumption is frequently not fully satisfied in image data.

$$f_c(x) = P(c) \prod_{i=1}^{n} P(x_i \mid c) \tag{18}$$

A representative artificial neural network-based technique used was the Multilayer Perceptron (MLP). MLP is made up of an input layer, an output layer, and one or more hidden layers that are connected by weights. By repeatedly updating the weights using a backpropagation learning algorithm, the model discovers the nonlinear relationships between texture features and tumor classes. MLP is used to assess how well neural networks can model the intricacy of MRI image textures.

$$f_c(x) = g(W_c x + b_c) \tag{19}$$

This study also used a multiclass classification approach to solve the multi-class classification problem. By breaking the problem down into multiple binary subproblems, this method makes it possible to apply binary classification algorithms, like SVM and Naive Bayes, to multiclass cases. The model can generate final class predictions based on the aggregation of results from several binary classifiers using popular strategies like one-vs-rest and one-vs-one.

$$f_c(x) = \sum_{j=1}^{m} f_{cj}(x) \tag{20}$$

The Random Forest algorithm was used as a classification technique based on ensemble learning. Several decision trees are built by Random Forest using randomly chosen feature subsets and data samples. Every tree offers a class prediction, and the majority vote from all trees determines the outcome. This method improves model stability against noise frequently found in MRI images, lowers the chance of overfitting, and enables Random Forest to capture intricate patterns.

$$f_c(x) = \frac{1}{T} \sum_{t=1}^{T} I(h_x(x) = c) \tag{21}$$

Performance metrics such as accuracy, sensitivity, and specificity were used to assess each classification algorithm. Three tumor type comparison scenarios were evaluated: glioma–meningioma, glioma–pituitary, and meningioma–pituitary. This method offers a thorough summary of each technique's efficacy in categorizing MRI images of brain tumors.

RESULT AND DISCUSSION

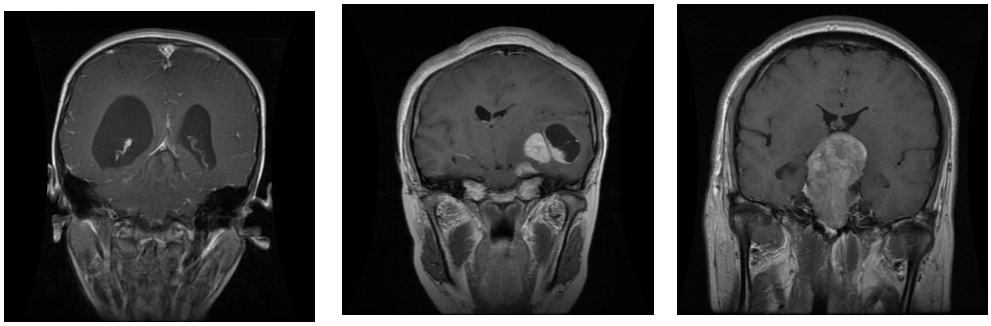

(a) (b) (c)

Figure 2. (a) MRI image of a patient with glioma tumor. (b) MRI image of a patient with meningioma tumor. (c) MRI image of a patient with a pituitary tumor.

The MRI pictures used in this study show a variety of brain tumor types with unique visual traits that represent variations in tissue structure and the degree of heterogeneity of each tumor (Figure 2). Lesion areas in glioma patients' MRI images show varying signal intensities. This pattern, especially in T2-weighted and FLAIR images, is typically linked to the infiltrative nature of gliomas, where tumor cells proliferate into surrounding brain tissue, producing complex intensity variations.

When compared to gliomas, meningiomas exhibit comparatively more uniform lesions with distinct borders on MRI images. Usually, these tumors show up as distinct extra-axial masses with a consistent contrast. These features produce more regular and consistent image textures because they reflect the localized growth pattern of meningiomas, which are typically non-infiltrative.

On the other hand, MRI pictures of pituitary tumors show comparatively smaller lesions confined to the sella turcica area. Pituitary tumors typically show little variation in signal intensity, though some cases may show contrast differences because of changes in the pituitary gland's structure or tissue composition. These tumors have distinct visual characteristics from gliomas and meningiomas due to their particular anatomical location.

These three tumor types' unique visual features show that MRI images contain rich texture information in addition to being a visual diagnostic tool. In image processing and machine learning-based classification, this data can be quantitatively extracted and used as discriminative features. As a result, the MRI pictures utilized in this investigation are regarded as representative for assessing how well classification techniques can distinguish between different types of brain tumors according to their texture features.

Table 1. Comparison of texture features between glioma and meningioma

Texture Feature	Glioma	Meningioma	Average	Rank
Mean	32.7794 ± 8.5878	43.3818 ± 14.0832	0.01	4
Standard Deveation	**38.3491 ± 5.799**	**46.6843 ± 7.8668**	**0.02**	**1**
Variance	1504.2705 ± 446.4253	2241.3061 ± 858.5758	0.016	2
Entropy	11.7322 ± 0.1978	11.7248 ± 0.3734	0.01	5
Skewness	1.2085 ± 0.3197	1.0723 ± 0.3401	0.006	11
Kurtosis	1.3422 ± 1.0702	0.7853 ± 0.9452	0.007	9
Contrast	47.1929 ± 15.0157	73.2865 ± 94.8413	0.009	6
Correlation	0.9835 ± 0.0055	0.9845 ± 0.0127	0.008	8
Energy	0.2602 ± 0.0915	0.2029 ± 0.0876	0.016	3
Homogenity	0.5981 ± 0.0924	0.5432 ± 0.1045	0.009	7

Short Run Emphasis	148874.5759 ± 31808.3844	158859.1193 ± 58789.6359	0.004	12
Long Run Emphasis	92137631.2927 ± 60344895.9222	46567959.9896 ± 82520925.6864	0.006	10
Grey Level Nonunformity	6179647876.6783 ± 3061556991.4574	4315738427.9212 ± 6278665727.4947	0.002	13
Run Length Nonunformity	21697742779.1054 ± 9275334765.7203	26841185911.6656 ± 57977205437.2584	0.001	14
Run Percentage	1 ± 0.0017	1 ± 0.0017	0	15

Standard deviation was found to be the most important feature in differentiating between glioma and meningioma based on the data in Table 1, which compares texture features between the two tumor types. In a nutshell, the standard deviation shows how much an MRI image's pixel intensity varies. This variation is more common in gliomas because of the tumor's irregular and infiltrative nature, which includes necrotic areas, edema, and variations in the tissue's cellular density. Meningiomas, on the other hand, typically have a more uniform intensity distribution due to their more localized and structured growth. Because of this, standard deviation is a powerful differentiator between meningioma and glioma (Stuart et al., 2019).

Beyond standard deviation, the ranking results in Table 1 reveal the relative contribution of all 15 texture features to the discrimination of glioma and meningioma. Variance was ranked second (average weight: 0.016), consistent with its mathematical relationship to standard deviation as it directly measures the spread of pixel intensities. Because gliomas are marked by greater tissue heterogeneity than meningiomas, variance captures this structural difference as a second highly discriminative first-order feature. Energy from the GLCM was ranked third (0.016), indicating that the concentration of gray-level co-occurrence pairs differs between the two tumor classes; the comparatively lower energy in meningioma (0.2029 ± 0.0876) versus glioma (0.2602 ± 0.0915) reflects a more varied spatial distribution of pixel intensities in meningioma tissue.

Mean intensity (rank 4; 0.01) and entropy (rank 5; 0.01) demonstrated moderate discriminative ability. Meningiomas showed a higher mean intensity (43.3818 ± 14.0832) compared to gliomas (32.7794 ± 8.5878), which may reflect the generally brighter appearance of extra-axial meningioma lesions in MRI. Entropy values were similar between the two classes (11.7322 vs 11.7248), yielding a low discriminative weight, suggesting that the overall randomness of pixel distribution is comparable for both tumor types. Contrast (rank 6; 0.009) and homogeneity (rank 7; 0.009) showed that meningioma images had higher contrast variation (73.2865 ± 94.8413 vs 47.1929 ± 15.0157) while glioma images had slightly higher homogeneity (0.5981 ± 0.0924 vs 0.5432 ± 0.1045), indicating differences in local pixel uniformity.

Correlation (rank 8; 0.008) and kurtosis (rank 9; 0.007) provided lower but still positive contributions. Correlation values were close between classes (0.9835 vs 0.9845), indicating comparable linear dependence in spatial gray-level relationships. Kurtosis was higher in glioma (1.3422 ± 1.0702) than meningioma (0.7853 ± 0.9452), reflecting a more peaked intensity histogram distribution in glioma images. Features derived from the GLRLM—Long Run Emphasis (rank 10; 0.006), skewness (rank 11; 0.006), Short Run Emphasis (rank 12; 0.004), Grey Level Non-uniformity (rank 13; 0.002), and Run Length Non-uniformity (rank 14; 0.001)—showed progressively lower discriminative weights, suggesting that run-length based texture patterns contribute less to separating glioma from meningioma in this dataset compared to first-order and co-occurrence features. Run Percentage was ranked last (rank 15; weight: 0) as both classes showed identical values (1 ± 0.0017), offering no class separation.

Table 2. Comparison of texture features between glioma and pituitary

Texture Feature	Glioma	Pituitary	Average	Rank

Mean	32.7803 ± 8.5883	49.428 ± 8.2598	0.021	7
Standard Deviation	38.3495 ± 5.7993	41.3984 ± 4.858	0.019	8
Variance	1504.2804 ± 1504.2804	1737.4062 ± 410.4264	0.016	9
Entropy	11.7322 ± 0.1978	12.0476 ± 0.2446	0.012	10
Skewness	1.2085 ± 1.2085	0.7958 ± 0.2675	0.021	6
Kurtosis	1.3422 ± 1.0702	0.6886 ± 0.9082	0.026	4
Contrast	47.1986 ± 15.0165	75.2499 ± 37.705	0.01	11
Correlation	0.9835 ± 0.0055	0.9775 ± 0.0115	0.01	12
Energy	0.2602 ± 0.0915	0.1064 ± 0.0772	0.043	1
Homogenity	0.5981 ± 0.0924	0.4024 ± 0.0853	0.042	2
Short Run Emphasis	148879.832 ± 31817.533	211183.5302 ± 64778.0702	0.006	13
Long Run Emphasis	92143343.4826 ± 60345804.5035	13635951.0319 ± 26959083.7365	0.031	3
Grey Level Nonunformity	6179155944.7788 ± 3060890603.1502	2111966499.3578 ± 2026469084.0438	0.023	5
Run Length Nonunformity	21698428110.7928 ± 9277876248.8439	46144655329.7639 ± 89685736594.5979	0.001	14
Run Percentage	1 ± 0.0017	1 ± 0.0017	0	15

The GLCM feature energy was found to be the most prevalent feature based on the data in Table 2, which contrasts gliomas and pituitary tumors. The degree of regularity in an image's pixel intensity patterns is represented by energy. In general, pituitary adenomas have more uniform and localized textures, which lead to more organized intensity patterns. Gliomas, on the other hand, have more erratic textures because of their infiltrative growth into the surrounding tissue. The energy values clearly show this variation in patterns. These results suggest that spatial information that cannot be obtained from histogram analysis alone can be captured by second-order features like GLCM. Energy is therefore a useful characteristic for differentiating between these two types of tumors (Haralick et al., 1973).

The idea that MRI texture reflects the biological features of tumors is supported by the difference in energy values between gliomas and pituitary tumors. While localized tumors display more consistent patterns, infiltrative tumors typically produce irregular texture patterns. This supports the use of texture analysis as a non-invasive method to comprehend variations in the structure of tumor tissue (Gallego-Ortiz & Martel, 2016).

The full ranking in Table 2 further clarifies the contribution of each feature. Homogeneity was ranked second (average weight: 0.042), close to energy, as pituitary tumors presented lower homogeneity values (0.4024 ± 0.0853) compared to gliomas (0.5981 ± 0.0924), reflecting the infiltrative nature of gliomas producing more locally uniform neighborhoods despite overall tissue heterogeneity. Long Run Emphasis was ranked third (0.031), with gliomas showing markedly higher values (92,143,343.48 ± 60,345,804.50) than pituitary tumors (13,635,951.03 ± 26,959,083.74), indicating that glioma images contain more runs of longer length, consistent with coarser and more irregularly extended tissue patterns.

Kurtosis (rank 4; 0.026) and Grey Level Non-uniformity (rank 5; 0.023) contributed moderately. Gliomas showed higher kurtosis (1.3422 ± 1.0702) than pituitary tumors (0.6886 ± 0.9082), indicating a more peaked intensity distribution in glioma. Grey Level Non-uniformity was higher in glioma (6,179,155,944.78 ± 3,060,890,603.15) than pituitary tumors (2,111,966,499.36 ±

2,026,469,084.04), suggesting greater variability in gray-level run distributions in glioma images. Skewness (rank 6; 0.021) and mean (rank 7; 0.021) showed that pituitary tumors had lower skewness (0.7958 ± 0.2675 vs 1.2085) but higher mean intensity (49.428 ± 8.2598 vs 32.7803 ± 8.5883), consistent with the anatomical brightness of pituitary region tissues in MRI. Standard deviation (rank 8; 0.019) and variance (rank 9; 0.016) contributed less for this tumor pair compared to the glioma–meningioma pair, as both tumor types showed relatively comparable intensity spread. Entropy (rank 10; 0.012), contrast (rank 11; 0.01), and correlation (rank 12; 0.01) offered minimal discrimination, while Short Run Emphasis (rank 13; 0.006), Run Length Non-uniformity (rank 14; 0.001), and Run Percentage (rank 15; 0) showed negligible or no discriminative power.

Table 3. Comparison of texture features between meningioma and pituitary

Texture Feature	Meningioma	Pituitary	Average	Rank
Mean	43.3821 ± 14.0837	49.4279 ± 8.2594	0.015	7
Standard Deviation	46.6844 ± 7.8669	41.3988 ± 4.8574	0.02	3
Variance	2241.3426 ± 858.5669	1737.416 ± 410.4403	0.016	6
Entropy	11.7248 ± 0.3734	12.0477 ± 0.2446	0.012	8
Skewness	1.0723 ± 0.3401	0.7958 ± 0.2675	0.019	4
Kurtosis	0.7854 ± 0.9452	0.6887 ± 0.9082	0.019	5
Contrast	73.2827 ± 94.84	75.2487 ± 37.6978	0.011	9
Correlation	0.9845 ± 0.0127	0.9775 ± 0.0115	0.01	10
Energy	0.2029 ± 0.0876	0.1064 ± 0.0772	0.029	2
Homogenity	0.5432 ± 0.1045	0.4024 ± 0.0853	0.032	1
Short Run Emphasis	158862.1845 ± 58793.4664	211172.6771 ± 64781.7518	0.005	11
Long Run Emphasis	46581652.9288 ± 82523567.6315	13704193.4428 ± 26923266.7418	0.003	13
Grey Level Nonunformity	4316550988.6319 ± 6278371385.2953	2111027463.6509 ± 2026462589.9095	0.003	12
Run Length Nonunformity	26833157720.608 ± 57962358833.2367	46145022068.6329 ± 89714605781.0344	0.001	14
Run Percentage	1 ± 0.0017	1 ± 0.0017	0	15

According to Table 3, which contrasts the texture characteristics of pituitary tumors and meningiomas, homogeneity was found to be the main differentiator. The degree of similarity between adjacent pixel intensities is reflected in homogeneity. Meningiomas may exhibit local variations, such as because of calcifications or particular vascular patterns, while pituitary adenomas frequently have relatively uniform internal structures. Because of these variations, the homogeneity values between the two tumor classes are consistently different (Waugh et al., 2015).

From a clinical standpoint, tissue homogeneity within a tumor is frequently linked to the degree of signal homogeneity. Therefore, variations in homogeneity values between pituitary tumors and meningiomas can give radiologists more information than just visual observation when evaluating lesion characteristics (Chu et al., 2016).

The full ranking from Table 3 shows that all 15 features contribute to varying degrees in separating meningioma from pituitary tumors. Energy was ranked second (average weight: 0.029), with meningioma showing higher energy values (0.2029 ± 0.0876) compared to pituitary tumors (0.1064 ± 0.0772), indicating that meningioma images contain more concentrated gray-level co-occurrence pairs,

reflecting their more structured lesion appearance. Standard deviation (rank 3; 0.02) and skewness (rank 4; 0.019) both showed that meningiomas had higher standard deviation (46.6844 ± 7.8669 vs 41.3988 ± 4.8574) and higher skewness (1.0723 ± 0.3401 vs 0.7958 ± 0.2675), reflecting greater pixel intensity variability and asymmetry in meningioma images compared to pituitary tumors.

Kurtosis (rank 5; 0.019) and variance (rank 6; 0.016) contributed similarly. Meningioma presented higher variance (2,241.3426 ± 858.5669 vs 1,737.416 ± 410.4403) and slightly higher kurtosis (0.7854 ± 0.9452 vs 0.6887 ± 0.9082) than pituitary tumors, further supporting the observation of greater intensity variation in meningioma tissue. Mean (rank 7; 0.015) and entropy (rank 8; 0.012) showed smaller differences: pituitary tumors had slightly higher mean intensity (49.4279 ± 8.2594 vs 43.3821 ± 14.0837) and entropy (12.0477 ± 0.2446 vs 11.7248 ± 0.3734). Contrast (rank 9; 0.011) and correlation (rank 10; 0.01) also contributed marginally, with both tumor types showing comparable values for these GLCM-derived features. The GLRLM features—Short Run Emphasis (rank 11; 0.005), Grey Level Non-uniformity (rank 12; 0.003), Long Run Emphasis (rank 13; 0.003), Run Length Non-uniformity (rank 14; 0.001), and Run Percentage (rank 15; 0)—consistently showed the lowest discriminative weights, indicating that run-length based features contributed minimally to distinguishing meningioma from pituitary tumors in this study.

Table 4. Comparison of classification methods for glioma and meningioma

Classification Method	Support Vector Machine	Naive Bayes	Multilayer Perceptron	Multiclass Classifier	Random Forest
TP	944	1128	952	990	1075
FP	356	172	348	310	225
TN	1084	505	1143	1091	1229
FN	216	795	157	209	71
Accuracy	78.00	62.81	80.58	80.04	**88.62**
Sensitivity	81.38	58.66	85.84	82.57	**93.80**
Spesificity	75.28	74.59	76.66	77.87	**84.53**

Table 5. Comparison of classification methods for glioma and pituitary

Classification Method	Support Vector Machine	Naive Bayes	Multilayer Perceptron	Multiclass Classifier	Random Forest
TP	1144	1072	1230	1220	1257
FP	156	228	70	80	43
TN	1169	1104	1240	1223	1264
FN	131	196	60	77	36
Accuracy	88.96	83.69	95.00	93.96	**96.96**
Sensitivity	89.73	84.54	95.35	94.06	**97.22**
Spesificity	88.23	82.88	94.66	93.86	**96.71**

Table 6. Comparison of classification methods for meningioma and pituitary

Classification Method	Support Vector Machine	Naive Bayes	Multilayer Perceptron	Multiclass Classifier	Random Forest

TP	1140	768	1169	1148	1236
FP	160	532	131	152	64
TN	1116	1088	1203	1167	1258
FN	184	212	97	133	42
Accuracy	86.77	71.38	91.23	89.04	**95.92**
Sensitivity	86.10	78.37	92.34	89.62	**96.71**
Spesificity	87.46	67.16	90.18	88.48	**95.16**

Random Forest consistently performed better than the other classification techniques, according to the testing results. The way Random Forest integrates several decision trees is the source of this benefit. This method increases the model's adaptability to complex variations in texture features within MRI images and nonlinear relationships (Breiman, 2001).

Noise from variations in equipment, acquisition parameters, or patient conditions frequently appears in MRI images. Because each decision tree is trained using distinct subsets of data and features, Random Forest is comparatively resilient to such circumstances. Errors from some trees can be offset by others through the majority voting mechanism, producing more consistent classification results (Díaz-Uriarte & De Andres, 2006).

Because the Naive Bayes method assumes feature independence, which is rarely met in MRI texture data, it tended to yield lower performance. While Multilayer Perceptron is sensitive to data size and weight initialization, SVM requires careful parameter selection for optimal performance. These elements clarify why Random Forest produced more reliable findings in this investigation (Mohsen et al., 2018).

Random Forest's strong potential for advancement in computer-aided diagnosis (CAD) systems for brain tumors is demonstrated by its high performance. Random Forest's accuracy is complemented by its ability to analyze each feature's contribution, which improves the interpretability of classification results and may boost clinicians' confidence in AI-based systems (Pereira et al., 2016).

Table 7. Classification data using Random Forest

Brain Tumors	**Accuracy**	**Sensitivity**	**Spesificity**
Glioma - Meningioma	88.62	93.80	84.53
Glioma - Pituitary	**96.96**	**97.22**	**96.71**
Meningioma - Pituitary	95.92	96.71	95.16

As shown in Table 7, the glioma–pituitary classification produced the best results among all comparison pairs because it reached 96.96% accuracy and 97.22% sensitivity and 96.71% specificity. The Random Forest model shows high performance in tumor type identification because its three evaluation metrics reach high values which help it detect both positive and negative cases. The system achieves superior results because multiple biological and radiological and algorithmic elements work together to enhance each other's performance.

The sella turcica serves as the primary location for pituitary tumor development because these tumors remain small while maintaining their restricted growth patterns. The specific characteristics of these tumors produce MRI images of pituitary tumors which show uniform texture patterns. The brain tissue shows different textures because gliomas develop throughout various brain areas while they spread through brain tissue to create multiple tissue changes. The strong difference between these two tumor types creates distinct texture patterns which become easily distinguishable through histogram and GLCM-based feature analysis of energy and homogeneity.

The anatomical location of pituitary tumors has well-defined boundaries which enables

researchers to extract the region of interest (ROI) with high precision. The quality of extracted features depends on stable and minimally ambiguous ROIs because they minimize the variation between different classes. The condition presents differently from meningiomas because these tumors maintain distinct borders yet they stick to dural structures and cortical edges which makes their texture more complex and their features more similar to other tumor types. Research studies have shown that machine learning-based MRI image classification needs both consistent tumor positions and similar tumor appearances to achieve better results.

Overall, the study's findings show that brain tumor types in MRI images can be successfully distinguished using a combination of first-order and second-order texture features. Due to their structural and biological differences, each tumor pair displays distinct dominant features. Random Forest is a dependable option for the classification of brain tumor MRI images, as evidenced by its consistent performance on all tests.

CONCLUSION

This study shows that combining Histogram, GLCM, and GLRLM texture features with machine learning algorithms can effectively perform MRI image classification for differentiating glioma, meningioma, and pituitary tumors. The most discriminative texture features varied for each tumor pair from a total of 3,900 MRI images analyzed: homogeneity for meningioma–pituitary, energy for glioma–pituitary, and standard deviation for glioma–meningioma. Random Forest consistently outperformed SVM, Naive Bayes, Multilayer Perceptron, and Multiclass Classifier during the classification stage, with high sensitivity and specificity in all testing scenarios and accuracies of 88.62% (glioma–meningioma), 96.96% (glioma–pituitary), and 95.92% (meningioma–pituitary). These results confirm that Random Forest is the most reliable method for handling the complexity and variation of MRI tumor texture features and holds strong potential for development as an objective and accurate computer-aided diagnostic system.

REFERENCE

Andono, P. N., T.Sutojo, & Muljono. (2018). Pengolahan Citra Digital. Penerbit Andi.

Astiningrum, M., Syulistyo, A. R., & Zakariya, M. A. (2020). Identifikasi Kualitas Biji Jagung Manis Layak Jual dari Warna dan Tekstur Menggunakan HSV dan Gray Level Run Length Matrix (GLRLM). JIP (Jurnal Informatika Polinema), 7(1), 37–44. https://doi.org/10.33795/jip.v7i1.439

Breiman, L. (2001). Random forests. Machine Learning, 45(1), 5–32.

https://doi.org/10.1023/A:1010933404324

Chu, A., Sehgal, C. M., & Greenleaf, J. F. (1990). Use of gray value distribution of medical images for tissue characterization. Ultrasound in Medicine & Biology, 16(6), 495–502. https://doi.org/10.1016/0301-5629(90)90007-9

Díaz-Uriarte, R., & De Andres, S. A. (2006). Gene selection and classification of microarray data using random forest. BMC Bioinformatics, 7, 3.

https://doi.org/10.1186/1471-2105-7-3

Gallego-Ortiz, C., & Martel, A. L. (2016). Quantitative MRI texture analysis of brain tumors. Magnetic Resonance Imaging, 34(5), 620–627.

https://doi.org/10.1016/j.mri.2016.02.004

Haralick, R. M., Shanmugam, K., & Dinstein, I. (1973). Textural features for image classification. IEEE Transactions on Systems, Man, and Cybernetics, SMC-3(6), 610–621. https://doi.org/10.1109/TSMC.1973.4309314

Heranurweni, S., Destyningtias, B., & Nugroho, A. K. (2018). Klasifikasi Pola Image Pada Pasien Tumor Otak Berbasis Jaringan Syaraf Tiruan (Studi Kasus Penanganan Kuratif Pasien Tumor Otak). Elektrika, 10(2), 37. https://doi.org/10.26623/elektrika.v10i2.1169

Kusuma, I. W. A. W., & Kusumadewi, A. (2020). Penerapan Metode Contrast Stretching, Histogram Equalization,dan Adaptive Histogram Equalization untuk Meningkatkan Kualitas Citra Medis MRI. SIMETRIS: Jurnal Teknik Mesin, Elektro dan Ilmu Komputer, 11(1), 1–10. https://doi.org/10.24176/simet.v11i1.3153

Laksono, P., Harliana, & Prabowo, T. (2023). Deteksi Tumor Otak Melalui Penerapan GLCM dan Naïve Bayes Classification. Jurnal Ilmiah Intech : Information Technology Journal of UMUS, 5(1), 41–48. https://doi.org/10.46772/intech.v5i1.1286

Maulida, N. S., Susanto, E., & Murniati, E. (2019). Prosedur Pemeriksaan Magnetic Resonance Imaging (MRI) Brain Perfusi dengan Metode Arterial Spin Labeling (ASL) pada Pasien Tumor. JRI (Jurnal Radiografer Indonesia), 2(1), 48–58. https://doi.org/10.55451/jri.v2i1.33

Mohsen, H., El-Dahshan, E. S. A., El-Horbaty, E. S. M., & Salem, A. B. M. (2018). Classification using deep learning neural networks for brain tumors. Future Computing and Informatics Journal, 3(1), 68–71.

https://doi.org/10.1016/j.fcij.2017.12.001

Pereira, S., Pinto, A., Alves, V., & Silva, C. A. (2016). Brain tumor segmentation using convolutional neural networks in MRI images. IEEE Transactions on Medical Imaging, 35(5), 1240–1251. https://doi.org/10.1109/TMI.2016.2538465

Salman, M., Kurniawan, R., Intan, B., & Santoso, B. (2025). Deteksi Dini Terhadap Penyakit Tumor Otak Menggunakan Citra Magnetic Resonance Imaging (MRI) dengan Pendekatan Deep Convolutional Neural Network. Jurnal Ilmiah Informatika, 10(1), 37–41. https://doi.org/10.35316/jimi.v10i1.37-41

Sofian, J., & Laluma, R. H. (2019). Klasifikasi Hasil Citra MRI Otak untuk Memprediksi Jenis Tumor Otak dengan Metode Image Threshold dan GLCM Menggunakan Algoritma K-NN (Nearest Neighbor) Classifier Berbasis Web. Jurnal Infotronik, 4(2). https://doi.org/10.32897/infotronik.2019.4.2.258

Stuart, A., Ord, J. K., & Arnold, S. (2019). Kendall's Advanced Theory of Statistics (Vol. 1). Wiley. https://doi.org/10.1002/9780470524042

Tarigan, H. B., Mulyantoro, D. K., & Rochmayanti, D. (2025). Deteksi Tumor Otak Pada Citra Magnetic Resonance Imaging (MRI) Brain dengan Metode Support Vector Machine (SVM). JURNAL NERS : Research & Learning in Nursing Science, 9(3), 4118–4135. https://doi.org/10.31004/jn.v9i3.46148

Wardhani, R., & Nafi'iyah, N. (2023). Identifikasi Tumor Otak Citra MRI dengan Convolutional Neural Network. Jurnal Informatika: Jurnal Pengembangan IT, 8(3), 213–219. https://doi.org/10.30591/jpit.v8i3.4985

Waugh, S. A., Purdie, C. A., Jordan, L. B., Vinnicombe, S., Lerski, R. A., & Thompson, A. M. (2016). Magnetic resonance imaging texture analysis classification of primary tumors. European Radiology, 26(2), 322–330.

https://doi.org/10.1007/s00330-015-3824-5

Zacharaki, E. I., Wang, S., Chawla, S., Yoo, D. S., Wolf, R., Melhem, E. R., & Davatzikos, C. (2009). Classification of brain tumor type and grade using MRI texture and shape in a machine learning scheme. Magnetic Resonance in Medicine, 62(6), 1609–1618.

https://doi.org/10.1002/mrm.22147